

THE CORRECT TREATMENT OF HARMONIC PRESSURE-FLOW BEHAVIOR IN MICROCHANNELS

Christopher J. Morris and Fred K. Forster *

Department of Mechanical Engineering
Campus Box 352600
University of Washington
Seattle, Washington 98195-2600

ABSTRACT

Advances in microfluidic technology give great potential for integrated systems with many components. Because continuum modeling is difficult even for simple systems, low-order modeling is essential to their design. Unsteady flow in microfluidic components such as channels and valves may require special treatment to achieve accurate low-order models of entire systems. One example is the fixed-valve micropump, in which the interaction between mechanical, electrical, and fluidic components produces maximum pump output at a resonant frequency near the corner frequency of the valves. In this frequency range the commonly-used value for fluid impedance was found to be in error by 30%, causing errors in predictions of pump membrane motion by as much as 300%. Proper treatment of the pressure-flow relations based on the exact solution of the Navier-Stokes equations for oscillatory flow corrected these deficiencies.

NOMENCLATURE

a channel half-width (m)
 A channel cross-sectional area (m²)
 b channel half-height (m)
 D_h channel hydraulic diameter $4A/P_e$ (m)
 f Darcy friction factor $4Po/Re$
 F force (N)
 i $\sqrt{-1}$

K sum of minor loss factors
 L channel length (m)
 \vec{n} outward unit normal vector
 P fluid pressure (Pa)
 P_e wetted perimeter (m)
 Po Pouiselle number See Eq. 3
 Re Reynolds number $\bar{V}D_h/\nu$
 Q volumetric flow (m³/s)
 \vec{V} velocity vector (m/s)
 \bar{V} average velocity (m/s)
 V volume (m³)
 w axial or z -component of velocity (m/s)
 \hat{Z} fluid impedance (kg/m⁴ s)
 α duct aspect ratio a/b
 η non-dimensional frequency parameter $b\sqrt{\omega/\nu}$
 μ fluid dynamic viscosity (Pa s)
 ν fluid kinematic viscosity (m²/s)
 ρ mass density (kg/m³)
 τ_w wall shear stress (Pa)
 $\bar{\tau}_w$ circumferential average wall shear stress $\int \tau_w ds/P_e$ (Pa)
 $()_e$ exact property
 $()_s$ simplified property
 $\hat{}$ complex amplitude
 $| |$ magnitude of a complex quantity

* Address correspondence to this author at the above address or to forster@u.washington.edu.

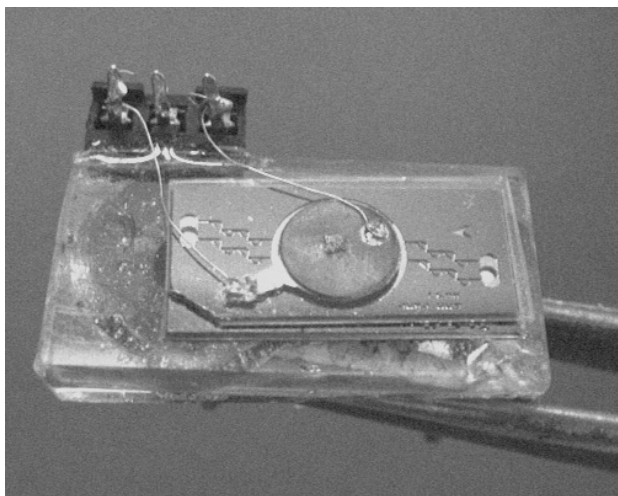


Figure 1. A FIXED-VALVE MICROPUMP WITH TWO PARALLEL, FOUR-ELEMENT, TESLA-TYPE INLET AND OUTLET VALVES AND A 6mm DIAMETER PUMP CHAMBER. VALVE CHANNELS ARE $114\mu\text{m}$ WIDE AND THE ETCH DEPTH OF VALVES AND CHAMBER IS $111\mu\text{m}$. THE PUMP IS DRIVEN BY A PIEZOELECTRIC ELEMENT MOUNTED OVER A FLEXIBLE PYREX MEMBRANE COVERING THE PUMP CHAMBER AND SEALING THE TOP SURFACE OF THE ETCHED SILICON SUBSTRATE.

INTRODUCTION

Micromachining technology enables microfluidic systems with many mechanical, electrical and fluidic components. Because continuum modeling is difficult even for simple systems, low-order modeling is essential for the design of such systems. For incompressible oscillating flow in a rigid channel a common low-order model is a fluid impedance \hat{Z} , which is the ratio of complex amplitudes of pressure drop $\widehat{\Delta P}$ to volume flow rate \widehat{Q} . The most common low-order representation is given by a series combination of a resistor R and inductor I ,

$$\hat{Z} = \frac{\widehat{\Delta P}}{\widehat{Q}} = R + i\omega I, \quad (1)$$

where often in the literature viscous and inertial effects are separately modeled by constant values of R and I , respectively.

For micropumps such as the one in Fig. 1, the interaction between electrical, mechanical, and fluidic components produces maximum pump output at a resonant frequency near the corner frequency of the valves (Forster et al., 1995). The valves for this pump are of fixed-geometry, etched in silicon using the DRIE process, and behave as fluid diodes to direct the flow. However, these valves exhibit relatively low diodicity, and for system design their behavior may be approximated by zero-mean

oscillatory flow through rigid channels and represented by fluid impedance \hat{Z} . A lower-order model describing the entire pump system with the valves modeled by constant values of R and I has been presented (Bardell et al., 1997). This approach results in a model having good agreement with a particular set of experimental data but of limited predictive value.

In this study we incorporate an improved method for obtaining the fluid impedance of a rectangular channel into our system model that does not utilize ad hoc values of R and I as described above. The method implemented in this study is based on the exact solution of the Navier-Stokes equations for oscillatory flow. At least one other study has addressed impedance modeling in a similar manner (D'Souza and Oldenburger, 1964). In that study viscosity was accounted for in rigid hydraulic pipes containing a compressible fluid, which was subject to pressure fluctuations about a mean pressure-driven steady flow. Results were compared to a simple inviscid "water-hammer" model. Here we study an incompressible fluid in rigid rectangular channels and fluctuations about a zero-mean flow.

METHODS

The methods used in this study are divided into three analytical and one experimental section. The analytical sections address the simplified impedance Z_s of a rectangular channel, the exact impedance Z_e of a rectangular channel, and the fully-developed flow assumption. The last section describes the experiments carried out. In all portions of this study gravitational effects are neglected since hydrostatic pressures are small compared to pressure differences caused by viscosity.

Simplified impedance for a rectangular channel

Simplified impedance is composed of lumped-parameter resistance and inductance values given by Eq. 1, where resistance and inductance are real constants. The commonly-used expression for simplified resistance, denoted in this study by R_s , is based on steady, viscous, fully-developed flow through a straight channel of arbitrary, constant cross-section and may be generalized in the form,

$$R_s = \frac{\mu L P_e^2 P_o}{8A^3}, \quad (2)$$

where P_o is the Poiseuille number defined by

$$P_o = \frac{2D_h \bar{\tau}_w}{\bar{V}\mu}. \quad (3)$$

For example, P_o is 16 for a circular cross-section and 24 for a two-dimensional slot, and for both cases the wall shear stress is

constant, $\overline{\tau_w} = \tau_w$ (White, 1991). With these values Eq. 2 reduces to the well-known steady-flow resistance formulas for those respective cases.

A general expression for simplified inductance I_s can be obtained by direct application of the momentum equation to unsteady, inviscid, fully-developed flow in a straight duct of arbitrary, constant cross-sectional area A . The momentum equation for a control volume (C.V.) consisting of the fluid in a straight duct between streamwise locations z_1 and z_2 yields the relation between the axial-direction force F_z and the rate of change of momentum in the control volume. For fully developed flow, i.e. velocity not a function of z ,

$$\begin{aligned} F_z &= \frac{d}{dt} \int_{C.V.} \rho w(x,y,t) dV \\ &\quad + \int_{C.V.} \rho w(x,y,t) \vec{\nabla}(x,y,t) \cdot \vec{n} dA \\ &= \rho \left[\frac{d}{dt} \int_A \int_z w(x,y,t) dz dA \right. \\ &\quad \left. - \int_{A_1} w^2(x,y,t) dA + \int_{A_2} w^2(x,y,t) dA \right]. \end{aligned} \quad (4)$$

For constant cross-sectional area, the integral over z in the first term can be replaced by the length L of duct considered, and the second and third terms cancel. In addition, for inviscid flow and not considering gravity, the net force is only due to the pressure difference over length L . Thus,

$$\Delta P A = \rho L \frac{d}{dt} \int_A w(x,y,t) dA \quad (5)$$

Noting that the integral of the velocity over the cross-sectional area is the volume flow rate Q ,

$$\Delta P = \frac{\rho L}{A} \frac{dQ}{dt}, \quad (6)$$

or

$$I_s = \frac{\rho L}{A}. \quad (7)$$

Equations 2 and 7 constitute the *simplified* expressions commonly found in systems textbooks (Rowell and Wormley, 1997) and applied to microdevice simulations (Bourouina and Grandchamp, 1996; Carmona et al., 1996). We emphasize again that Eq. 2 is derived for *steady, viscous* flow, while Eq. 7 is derived from *unsteady, inviscid* flow. Thus, when used together to obtain the fluid impedance according to Eq. 1 they represent an ad hoc, inconsistent approach.

For a rectangular channel of width $2a$ and height $2b$,

$$Po = \frac{24}{(1 + \alpha)^2} \left[1 - 6 \sum_{n=0}^{\infty} \frac{\alpha \tanh(p_n/\alpha)}{p_n^5} \right]^{-1}. \quad (8)$$

From Eqs. 2 and 8,

$$R_s = \frac{3\mu L}{4\alpha^3 b^4} \left[1 - 6 \sum_{n=0}^{\infty} \frac{\alpha \tanh(p_n/\alpha)}{p_n^5} \right]^{-1} \quad (9)$$

where $p_n = (2n + 1)\pi/2$. Equations 8 and 9 are consistent with the velocity field solution in a rectangular duct given by (White, 1991). Using Eq. 7 for a rectangular duct of width $2a$ and height $2b$, we obtain

$$I_s = \frac{\rho L}{4\alpha b^2} \quad (10)$$

For harmonic flow in a rectangular duct Eqs. 9 and 10 yield a simplified hydraulic impedance according to Eq. 1.

Exact impedance in a rectangular channel

An exact expression for impedance \hat{Z}_e can be derived directly from the solution of the Navier-Stokes equations for oscillatory flow in a duct of any constant cross-sectional area for which a closed-form velocity solution exists. We present here the derivation of the exact impedance for a rectangular duct.

The solution for the harmonic velocity field $w(x,y,t) = \hat{w}(x,y) \exp(i\omega t)$ for fully-developed oscillatory flow in a rectangular duct driven by a harmonic driving pressure difference $\Delta P = \hat{\Delta P} \exp(i\omega t)$ is given in (Drake, 1965),

$$\begin{aligned} \hat{w}(x,y) &= \frac{\hat{\Delta P}}{L} \frac{4b^2}{\pi\mu} \sum_{n=0}^{\infty} \left[\frac{(-1)^n}{(2n+1)q_n^2} \right. \\ &\quad \left. \times \left(1 - \frac{\cosh(q_n x/b)}{\cosh(q_n \alpha)} \right) \cos\left(\frac{(2n+1)\pi y}{2b}\right) \right], \end{aligned} \quad (11)$$

where

$$q_n = \sqrt{i\eta^2 + \frac{(2n+1)^2}{4}\pi^2}. \quad (12)$$

At least two other authors have published solutions for flow in a rectangular channel due to a periodic driving pressure (Fan and Chao, 1965; O'Brien, 1975). It should be noted that (O'Brien,

1975, Eq. (8) is dimensionally inconsistent. Our derivation yielded $W_1^* = 1/(-i\eta^2)$. With that correction, all three solutions were numerically evaluated using Matlab (v5.3, The Mathworks, Inc, Natick, MA) and gave the same impedance at frequencies above the corner frequency. However, at lower frequencies, the corrected formula in (O'Brien, 1975) exhibited numerical instabilities in the infinite series terms, so that formula was not used. Also, the formula in (Fan and Chao, 1965) was more computationally intensive because of a double summation.

The complex volume flow rate \hat{Q} was computed by integrating Eq. 11 over the cross-sectional area:

$$\hat{Q} = \frac{\widehat{\Delta P} 32b^4}{L \mu\pi^2} \sum_{n=0}^{\infty} \left[\frac{1}{(2n+1)^2 q_n^2} \left(\alpha - \frac{\tanh(q_n \alpha)}{q_n} \right) \right] \quad (13)$$

where $Q(t) = \hat{Q} \exp(i\omega t)$. Finally, using Eq. 1, we obtain

$$\hat{Z}_e = \frac{\mu L \pi^2}{32b^4} \left[\sum_{n=0}^{\infty} \frac{1}{(2n+1)^2 q_n^2} \left(\alpha - \frac{\tanh(q_n \alpha)}{q_n} \right) \right]^{-1} \quad (14)$$

With the above expression the exact resistance and inductance are given by

$$R_e = \text{Re}[Z_e] \quad I_e = \text{Im}[Z_e]/\omega. \quad (15)$$

Fully-developed flow considerations

In order to investigate the accuracy of the simplified and exact models of fluid impedance, both of which are based on fully developed flow, an experiment that also reflects the conditions of fully-developed flow is needed. The experiment must be designed to minimize additional pressure losses from entry and exit effects. The steady flow pressure drop ΔP in a channel may be represented by (White, 1994)

$$\Delta P = \left[K + f \left(\frac{L}{D_h} \right) \right] \frac{1}{2} \rho \bar{V}^2. \quad (16)$$

The quantity inside the square brackets gives insight into whether minor losses (such as entry or exit effects) may be neglected. If the quantity $f(L/D_h)$ is large compared to total minor loss factor K , then the laminar flow solution (used to determine the friction factor f) may be used to accurately predict the pressure drop in the channel. This is true at low Re. However, K becomes more significant as Re increases, and ΔP approaches a \bar{V}^2 relationship. By plotting Eq. 16 with $K = 2.3$ and with $K = 0$, the behavior of ΔP with increasing \bar{V} can be investigated with and without minor losses. The value for K was obtained from (Shah and London, 1978) who summarizes experimental data in a rectangular duct with $\alpha = 1$, from which $K_{\text{entry}} = 1.3$ can be deduced; and (White, 1994) who gives $K_{\text{exit}} = 1$.

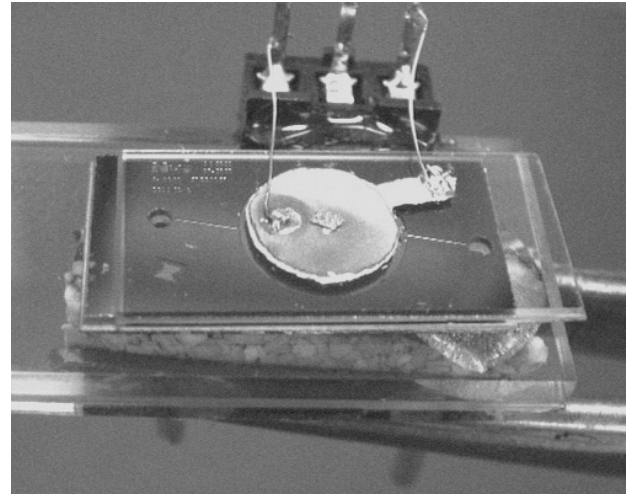


Figure 2. A 6 mm DIAMETER CHAMBER WITH 120 μm WIDE STRAIGHT CHANNELS ON EACH SIDE. ETCH DEPTHS FOR THREE DIFFERENT DEVICES STUDIED RANGED FROM 115 μm TO 148 μm . THE DEVICE WAS IDENTICAL IN FABRICATION TO THE PUMP SHOWN IN FIG. 1 EXCEPT THE VALVES (NON-LINEAR FLUID ELEMENTS) ARE REPLACED WITH STRAIGHT CHANNELS.

Experiments

Three devices like the one shown in Fig. 2 were used to investigate the effects of using Z_s and Z_e on model predictions. The device was identical in fabrication to the pump shown in Fig. 1 except the valves are replaced with straight channels. A 6 mm diameter chamber with 120 μm wide x 2240 μm long channels located on opposite sides of the chamber was etched in silicon using DRIE techniques. The etch depth was measured in the chamber using an optical interference measurement system (Fotonic MTI-2000, MTI Instruments, Albany, New York). A Pyrex cover was anodically bonded to the top, and a 5 mm dia. x 190 μm thick piezoelectric actuator was glued on the Pyrex using electrically-conductive epoxy. Holes were drilled through the silicon to allow inlet/outlet connections.

The relations given in this study for straight, rectangular channels were used to calculate R and I , assuming the flow was fully-developed throughout the channel length. Equation 16 was applied in a quasi-steady sense to oscillatory flow, and was used to determine the maximum peak Reynolds number for which Eq. 14 applied. To help validate Eq. 16, a steady flow test was performed using one of the straight-channel devices and a syringe pump (Model 200, KD Scientific, Boston, Massachusetts). The pressure drop through the device was measured with a water column for pressures below 10 kPa, and with a pressure transducer (EPI-127, Entran Sensors & Electronics, Fairfield, New Jersey) for pressures above 10 kPa. The resulting pressure drop

was divided by two for ΔP through a single channel, assuming each channel experienced the same entry and exit effects.

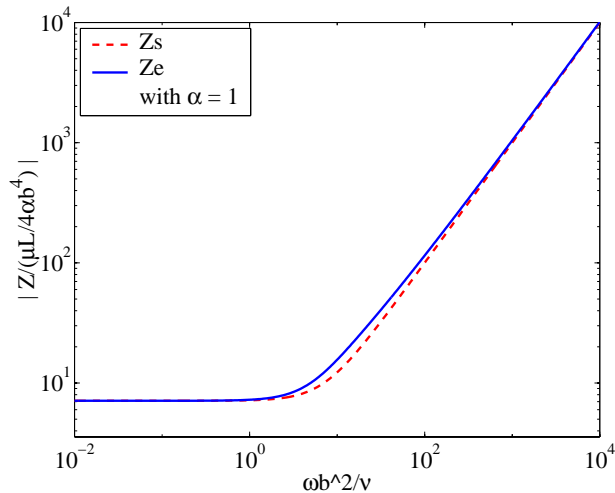


Figure 3. NON-DIMENSIONAL HYDRAULIC IMPEDANCE MAGNITUDE VS. NON-DIMENSIONAL FREQUENCY FOR A RECTANGULAR CHANNEL OF WIDTH $2a$ AND HEIGHT $2b$, WITH ASPECT RATIO $\alpha = 1$. MAGNITUDES FOR SIMPLIFIED IMPEDANCE $|Z_s|$ AND THE EXACT IMPEDANCE $|Z_e|$ GIVEN BY EQ. 14 ARE SHOWN.

To investigate the effect of the discrepancies between Z_s and Z_e , we modeled the chamber/straight-channel system shown in Fig. 2, similar to what we have done for fixed-valve micropumps (Bardell et al., 1997). A linear system model was implemented in Matlab. The finite element method in (Morris and Forster, 2000) was used to obtain values for mechanical parameters. Fluid parameters were calculated using Eqs. 9 and 10 for Z_s , and Eq. 14 for Z_e , with water at 25°C as the working fluid. The operating frequency for Eq. 14 was taken as the experimental resonant frequency. Chamber capacitance was modeled as a volumetric bubble fraction of air at 1 atm, and was adjusted so that the resonant frequency from the model using Z_e matched the resonant frequency of the experimental data. The same volumetric bubble fraction was used for all three devices. Frequency response data were gathered for the membrane centerline velocity using a laser vibrometer (Model OVF 302, Polytec, Waldbronn Germany) from the three chamber/straight-channel devices at low enough Reynolds number to neglect additional entry/exit losses. These data were compared to the system model predictions using Z_s and Z_e .

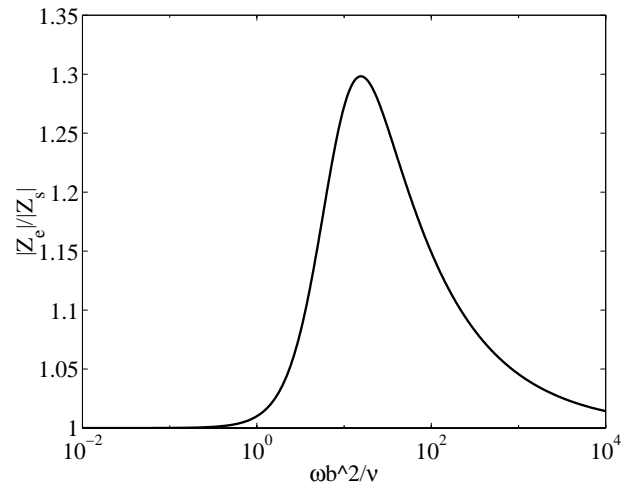


Figure 4. MAGNITUDE OF THE EXACT HYDRAULIC IMPEDANCE $|Z_e|$ RELATIVE TO THE SIMPLIFIED VALUE $|Z_s|$, VS. NON-DIMENSIONAL FREQUENCY FOR A RECTANGULAR CHANNEL, WITH ASPECT RATIO $\alpha = 1$. THE SAME INFORMATION IS CONTAINED IN THE IMPEDANCE PLOT OF FIG. 3, BUT HERE THE DIFFERENCE BETWEEN $|Z_e|$ AND $|Z_s|$ IS MORE QUANTITATIVELY EVIDENT.

RESULTS AND DISCUSSION

Figures 3 and 4 show there are significant differences (as much as 30%) between $|Z_s|$ and $|Z_e|$ for a rectangular duct, most notable near the corner frequency, i.e. the frequency at which the low and high frequency asymptotes intersect. The simplified impedance yields satisfactory results at low or high frequencies, but near the corner frequency the physics of oscillatory flow are too complex to be captured by the two constant lumped-parameters, R_s and I_s . Figure 5 shows the exact resistance and inductance using Eq. 15, relative to the constant, simple values R_s and I_s using Eqs. 9 and 10. Even though the largest differences are at high and low frequencies for R and I , respectively, R and I are almost insignificant contributions to impedance at those respective high and low frequencies. Their combined effect on impedance is greatest around the corner frequency, and several orders of magnitude beyond that frequency.

In order to use the exact impedance relation given in Eq. 14, the fully-developed flow condition had to be satisfied. Steady pressure drop vs. flow data were taken for a test device, and the results are shown in Fig. 6 along with predictions using Eq. 16. The figure shows a significant departure from the fully-developed flow assumption ($K = 0$) at $Re > 50$ for this channel length. So, at $Re < 50$, entry and exit effects could be safely neglected.

The membrane centerline velocity frequency response is shown in Fig. 7 for two devices whose etch depths were mea-

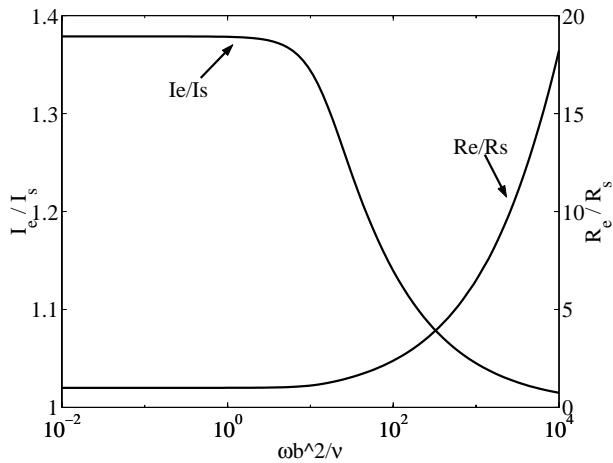


Figure 5. EXACT RESISTANCE R_e AND INDUCTANCE I_e OF A RECTANGULAR CHANNEL WITH $\alpha = 1$, RELATIVE TO SIMPLE RESISTANCE R_s AND INDUCTANCE I_s PLOTTED AS A FUNCTION OF NON-DIMENSIONAL FREQUENCY, η^2 .

sured to be $114\mu\text{m}$ and $115\mu\text{m}$, respectively. Also shown are model predictions for an etch depth of $115\mu\text{m}$ ($\alpha = 1.04$), based on Z_s and Z_e . A volumetric bubble fraction of 3×10^{-4} was used, and the predicted Re based on the RMS peak flow velocity in the channels at device resonance was 42. The actuation was 2V zero-to-peak. Figure 8 shows frequency response data and model predictions for a third device, whose etch depth was measured to be $148\mu\text{m}$ ($\alpha = 1.23$). The same bubble fraction was used, and the predicted Re based on RMS values of peak flow velocity was 50 at the same driving voltage. Because the channel depth was the only difference between the calculations for both figures, the data clearly show the improvement of using the exact impedance Z_e over the simplified R_s and I_s . The membrane velocity amplitude based on Z_s is 200 to 300% higher than measured, while calculations based on Z_e are in good agreement.

The method discussed in this study could also be applied to the pump in Fig. 1, except that computational fluid dynamics (CFD) is needed to determine R_e and I_e , because a closed-form solution does not exist for such a complicated geometry. Still, the principles in this study are vital to determining *how* to use the CFD method in obtaining R and I . Determining R from a steady flow simulation and I from Eq. 7 would be computationally efficient, but would only produce *simplified* values that would not apply over all frequencies, especially in the vicinity of the corner frequency. The more accurate method is harmonic CFD analysis at the desired frequency.

We conclude that proper handling of fluid resistance and inductance is essential to accurate transient low-order modeling.

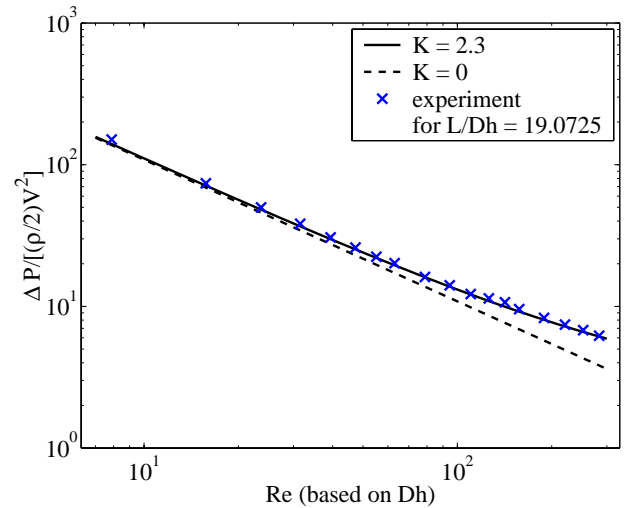


Figure 6. NON-DIMENSIONAL PRESSURE DROP VS. STEADY FLOW REYNOLDS NUMBER Re FOR A DEVICE LIKE THE ONE SHOWN IN FIG. 2, WITH AN ETCH DEPTH OF $115\mu\text{m}$, PLOTTED ON A LOG SCALE. PREDICTIONS WERE BASED ON EQ. 16. THE FIGURE SHOWS THAT IN A QUASI-STEADY SENSE, ADDITIONAL RESISTANCE DUE TO ENTRY/EXIT LOSSES MAY BE NEGLECTED AT LOW Re .

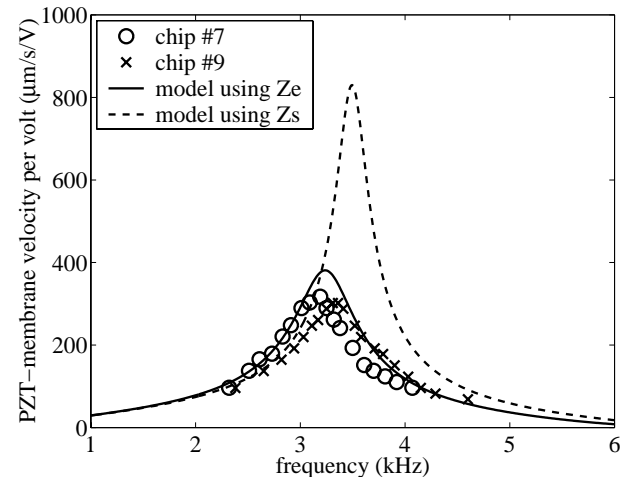


Figure 7. MEMBRANE VELOCITY FREQUENCY RESPONSE FOR TWO REALIZATIONS (LABELED AS CHIPS #7 AND #9) OF THE CHAMBER/CHANNEL SYSTEM SHOWN IN FIG. 2, AND COMPARISON WITH MODEL PREDICTIONS BASED ON SIMPLIFIED AND EXACT IMPEDANCE, Z_s AND Z_e . THE ETCH DEPTHS WERE 114 AND $115\mu\text{m}$ ($\alpha = 1.04$) FOR BOTH DEVICES, SO THE DATA IS SHOWN COMPARED TO THE SAME MODEL PREDICTIONS.

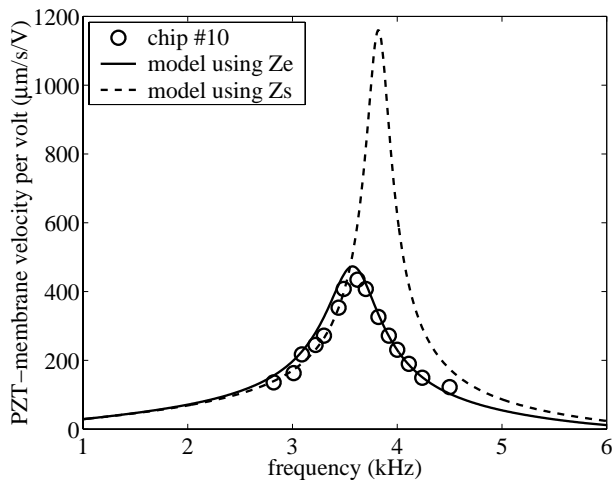


Figure 8. MEMBRANE VELOCITY FREQUENCY RESPONSE FOR ONE REALIZATION (LABELED AS CHIP #10) OF THE CHAMBER/CHANNEL SYSTEM SHOWN IN FIG. 2, AND COMPARISON WITH MODEL PREDICTIONS BASED ON SIMPLIFIED AND EXACT IMPEDANCE, Z_s AND Z_e . THE ETCH DEPTH WAS $148\mu\text{m}$ ($\alpha = 1.23$). THE PREDICTED REYNOLDS NUMBER BASED ON RMS VALUES OF FLOW VELOCITY IN THE CHANNELS AT DEVICE RESONANCE WAS 50. SHOWN IS GOOD AGREEMENT WITH EXPERIMENT WHEN THE EXACT FORM OF IMPEDANCE Z_e IS UTILIZED, AND OVER-PREDICTION BY 200 TO 300% FOR THE COMMONLY-USED METHOD BASED ON Z_s .

ACKNOWLEDGMENT

This work was partially supported by DARPA Microflumes Program contract N66001-97-C-8632, DARPA Composite CAD Program contract F30602-98-2-0151, and a graduate fellowship from the NASA Space Grant.

REFERENCES

- Bardell, R., Sharma, R., Forster, F. K., Afromowitz, M. A., and Penney, R. (1997). Designing high-performance micropumps based on no-moving-parts valves. In Lin, L., Goodson, K. E., et al., editors, *Micro-Electro-Mechanical Systems (MEMS), ASME International Mechanical Engineering Congress and Exposition (Dallas)*, volume DSC-234/HTD-354, pages 47–53, New York. ASME.
- Bourouina, T. and Grandchamp, J. (1996). Modeling micropumps with electrical equivalent networks. *J. Micromech. Microeng.*, 6(4):398–404.
- Carmona, M. et al. (1996). Dynamic simulations of micropumps. *J. Micromech. Microeng.*, 6:128–130.
- Drake, D. G. (1965). On the flow in a channel due to a periodic pressure gradient. *Quarterly Journal of Mechanics and*

Applied Mathematics, 18(1):1–10.

D'Souza, A. F. and Oldenburger, R. (1964). Dynamic response of fluid lines. *Trans. ASME: Journal of Basic Engineering*, pages 589–98.

Fan, C. and Chao, B.-T. (1965). Unsteady, laminar, incompressible flow through rectangular ducts. *ZAMP*, 16:351–360.

Forster, F., Bardell, R., Afromowitz, M., and Sharma, N. (1995). Design, fabrication and testing of fixed-valve micropumps. In Wiggert, D. C. et al., editors, *Proceedings of the ASME Fluids Engineering Division, ASME International Mechanical Engineering Congress and Exposition (San Francisco)*, volume 234, pages 39–44, New York. ASME.

Morris, C. J. and Forster, F. K. (2000). Optimization of a circular piezoelectric bimorph for a micropump driver. *J. Micromech. Microeng.*, 10:1–7.

O'Brien, V. (1975). Pulsatile fully developed flow in rectangular channels. *Journal of the Franklin Institute*, 300(3):225–30.

Rowell, D. and Wormley, D. N. (1997). *System Dynamics: An Introduction*. Upper Saddle River.

Shah, R. K. and London, A. L. (1978). *Laminar Flow Forced Convection in Ducts: A Source Book for Compact Heat Exchanger Analytical Data*. Academic Press.

White, F. M. (1991). *Viscous Fluid Flow*. McGraw-Hill, Inc., New York, 3rd edition.

White, F. M. (1994). *Fluid Mechanics*. McGraw-Hill, 3rd edition.